ADVANCED ELECTRONIC MATERIALS
www.advelectronicmat.de

Engineering Efficient p-Type TMD/Metal Contacts Using Fluorographene as a Buffer Layer

Tiziana Musso, Priyank V. Kumar, Jeffrey C. Grossman, and Adam S. Foster*

P-type transistors based on high work function transition metal dichalcogenide (TMD) monolayers such as MoS_2 are to date difficult to produce, owing to the strong Fermi level pinning at the semiconductor/contact metal interfaces. In this work, the potential of halogenated graphenes is demonstrated as a new class of efficient hole injection layers to TMDs such as MoS_2 and WSe_2 by taking fluorographene (or GF) as a model buffer layer. Using first-principles computations, two commonly obtained GF stoichiometries, C_2F and CF, have been studied as buffer layers between MoS_2 and Pt. In particular, for high work function TMDs such as MoS_2, it has been shown that C_2F forms an ohmic contact, while CF leads to a significant p-SBH value. On the other hand, for low work function TMDs such as WSe_2, both C_2F and CF lead to p-type ohmic contacts. This analysis shows that the ability of these buffer layers to form p-type contacts depends crucially on the charge redistribution at the GF/metal interface, which is dictated by their chemical interaction and equilibrium geometry. The fundamental electronic structures between the different semiconductor/insulator/metal interfaces which are part of this study have also been investigated.

1. Introduction

Transition metal dichalcogenides (TMDs) are layered 2D materials with many interesting electronic and optical properties. For example, MoX_2 and WX_2 (where X represents the chalcogen) have a band gap that is indirect in the bulk form, but becomes direct for monolayers.[1–6] Furthermore, monolayer TMDs are structurally stable and largely lack dangling bonds. The production processes of TMDs are currently well established, ranging from top-down exfoliation of the bulk material using mechanical exfoliation, solution-based approaches and the bottom-up synthesis methods using chemical vapor deposition.[7,8]

TMDs have gained significant importance as excellent candidates for nanoelectronic applications.[9,10] MoS_2 is one of the most commonly studied TMD in this regard, which demonstrates a high mobility (in the range 1–50 cm^2 V^{-1} s^{-1} at room temperature[11,12]), comparable to that of silicon. In addition, field-effect transistors (FETs) based on MoS_2 show low power dissipation[1] and efficient control over switching,[2] leading to widespread research interest in this topic.

While these properties are certainly encouraging, one major limitation of such FETs is that the carrier transport in the semiconductor channel is mostly electron-mediated,[13] resulting in n-type FETs (n-FETs). Despite attempts to employ high work-function metal contacts to obtain hole-based transport, the resulting devices have instead widely shown n-character.[13] This intrinsic behavior of the unmodified MoS_2-metal interface hinders the construction of fully integrated circuits,[7] because of the difficulty in obtaining a CMOS (complementary metal oxide semiconductor) device, where the building block of logic gates and digital circuits require both n- and p-type MOS architectures.

The fabrication of p-FETs based on monolayer MoS_2 is challenging[13] because of a particular interfacial phenomenon between the TMD and the metal contact, namely Fermi level pinning.[14,15] It is commonly believed that the interfacial gap states between MoS_2 and the metal contacts are responsible for pinning the Fermi level close to the conduction band, even upon using a high work-function metal. These gap states may be surface states (Bardeen's theory), metal-induced gap states (MIGS) or defect/disorder-induced gap states.[14,15] Guo, Francois and co-workers[16,17] consider the MIGS theory the best candidate to explain the origin of the gap states. A different point of view is assumed by McDonnell et al.,[18,19] wherein they attribute the difficulty in producing hole-based MoS_2 devices to the intrinsic low work-function defects present in MoS_2, responsible for the variability of electronic properties across the samples. These native defects such as vacancies present in MoS_2 and other TMDs like WSe_2 may actually result in variations of the TMDs work function, as observed in experiments.[20]

Dr. T. Musso,[+] Prof. A. S. Foster
COMP, Department of Applied Physics
Aalto School of Science
PO Box 11100, FI-00076 Aalto, Finland
E-mail: tiziana.musso@chem.uzh.ch
Dr. P. V. Kumar
Optical Materials Engineering Laboratory
ETH Zürich
Switzerland
Prof. J. C. Grossman
Department of Materials Science and Engineering
Massachusetts Institute of Technology
Cambridge, MA 02139, USA
Prof. A. S. Foster
Division of Electrical Engineering and Computer Science
Kanazawa University
Kanazawa 920-1192, Japan
[+]Present address: Department of Chemistry, University of Zürich, Winterthurerstrasse 190, CH-8057 Zürich, Switzerland

In memory of Tullia and Hiriyannaiah

DOI: 10.1002/aelm.201600318

One way to enhance the hole injection efficiency is to heavily dope the semiconductor in the contact region,[21,22] but it is difficult to locally control the doping, that could eventually deteriorate with time.[23] An alternative solution would be to insert a buffer layer between the semiconductor and the metal, thereby suppressing the interface states and de-pinning the Fermi level. Such a buffer layer has to be sufficiently thin in order to avoid the formation of a large barrier for the charge carriers to tunnel across.[21] Toward this end, substoichiometric molybdenum trioxide (MoO_x, $x < 3$)[13] and NbS_2[21] have been proposed as efficient hole-injection layers. It should be considered that depositing MoO_3 requires complex high temperature evaporation and deposition techniques in high vacuum, while monolayer NbS_2 is yet to be fabricated.[24] Along these lines, in our previous theoretical work[25] we proposed graphene oxide (GO) as an efficient buffer layer, leading to low hole Schottky barrier heights (denoted as p-SBHs) when it is fully functionalized with epoxy groups. Recent experiments have confirmed our result, wherein GO has been employed to induce hole injection and hole doping in WSe_2-based devices.[26]

Based on these results for GO, we explored other functionalized graphene derivatives that could be used as hole-injection layers. To this end, an important class of covalently modified graphene-derivatives are halogenated graphenes that, thanks to the halogens attached to the graphene plane, exhibit a wide range of interesting properties.[27] From our preliminary calculations, we noted that such halogenated graphenes could exhibit work function values higher than that of GO, and therefore could perform better when compared to GO (see Figure S1, Supporting Information). Although graphene functionalized with carbonyl functional groups gives the highest work-function according to our simulations, it is challenging to produce a solely carbonyl-functionalized graphene layer owing to stability issues, in contrast to GF. This happens because the reduction of graphene oxide invariably results in the formation of a mix of functional groups including carbonyl, ether, unreduced epoxy, and hydroxyl groups on the graphene plane.[28]

In this work, we demonstrate the potential of one such halogenated graphene, namely fluorographene or graphene fluoride (abbreviated GF henceforth), which is structurally stable at ambient conditions, thermally and chemically robust,[29] and whose synthesis procedures are relatively well-established among the family of halogenated graphenes.[30] GF as a monolayer has only been synthesized first in 2010.[27] The easiest production method is mechanical exfoliation of pristine graphite fluoride, in a similar way to getting graphene from graphite, but large-scale applications are di cult. GF can also be prepared from graphene fluorination, either at high temperature (leading to C_2F and CF stoichiometry) or at room temperature, with a gaseous mixture of fluorine and HF (resulting in C_xF ($x < 2$) structures)[31] or xenon difluoride.[32] In this last case, the maximum fluorination can be 25% for single-side exposure (C_4F) or 100% for double-sided exposure (CF), implying that the actual GF stoichiometry depends on the experimental conditions and the fluorination source.[31]

Using first-principles computations, we study two commonly obtained GF stoichiometries, C_2F and CF, as buffer layers between MoS_2 and Pt. We demonstrate that C_2F forms an ohmic contact with monolayer MoS_2, while CF leads to a significant p-SBH value. Our result reveals that an increase in the halogen concentration is not necessarily an ideal direction to pursue as one might intuitively expect due to an increase in work function going from C_2F to CF. We rationalize this result by studying the relevant interfaces in detail. Finally, we extend our results to other TMDs and metal systems, such as WSe_2 and Co. These studies could help design improved TMD-based p-type FETs and are also useful in elucidating the fundamental electronic structure between the different interfaces considered here.

2. Structural Models and Computational Details

We consider two GF stoichiometries in our simulations, i.e., with 50% fluorine coverage and full coverage, namely C_2F and CF, respectively. Concerning the positions of fluorine atoms on the carbon plane, initially two possible arrangements were proposed,[33] while later work identified four stable configurations,[34] although it should be noted that these configurations differ in stability by a small energy value (by ≈0.07 eV/atom).[31,33,34] Further, ab initio calculations disagree with experiments for several properties, concerning for example, the band gap and the Young's modulus of GF. These discrepancies have been ascribed to possible different or mixed fluorine configurations on the graphene plane or to the intrinsic presence of defects in the GF samples.[27,34] Based on the reasons mentioned above, we have decided to model GF by randomly attaching the fluorine atoms above and below the graphene plane, as shown in **Figure 1**.[25]

Our unit cell consists of a GF buffer layer (C_2F or CF) sandwiched between the TMD monolayer and the metal slab, as shown in Figure 1. We have chosen platinum as an ideal high work function contact metal to make p-type TMDs, with the (111) surface facing the buffer layer. By analyzing the surface energy versus the number of layers (see Figure S2, Supporting Information), we find that six Pt layers are a good approximation to model the metal slab.[18] Regarding the stacking between GF and the semiconductor, we have adopted the so called TM configuration, wherein before structural relaxation, the

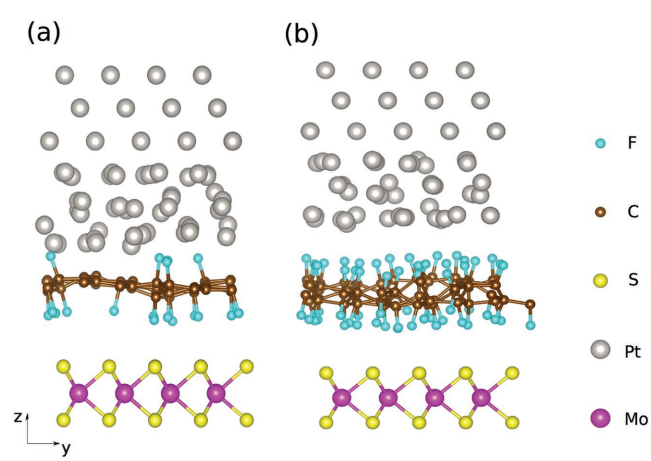

Figure 1. Example of relaxed supercells (lateral view) formed by MoS_2, GF, and Pt. In (a), GF is present as C_2F, while in (b) as CF.

carbon atom of GF sits above the Mo atom of MoS_2.[35] Ma et al. demonstrated[35] the equivalence of the TM to the TS configuration, where a C atom sits above a S atom. For coherence with our previous work,[25] we have chosen the TM arrangement.

We have used the minimum lattice mismatch criteria to obtain the dimensions of the supercell containing the three materials. The metal and the GF monolayer have been strained to match the semiconductor's lattice parameter, in order to avoid large band gap modifications in the TMD.[25] The supercell contains a (5 × 5) layer of graphene for modelling GF (2 C atoms per unit cell), a (4 × 4) layer of MoS_2 (1 Mo and 2 S atoms per unit cell) and a (4 × 4) layer of Pt slab (6 Pt atoms per unit cell). In this way the graphene plane is expanded by 3.29%, while the Pt unit cell is expanded by 9.72%. Although the Pt is strained by a considerable amount in this configuration, using such a construct, we computed a p-SBH value of 0.70 eV at the MoS_2/Pt interface (without the buffer layer), in good agreement with the value of 0.77 eV obtained by Gong et al., showing that the strain in Pt does not affect the conclusions drawn in this paper.[14]

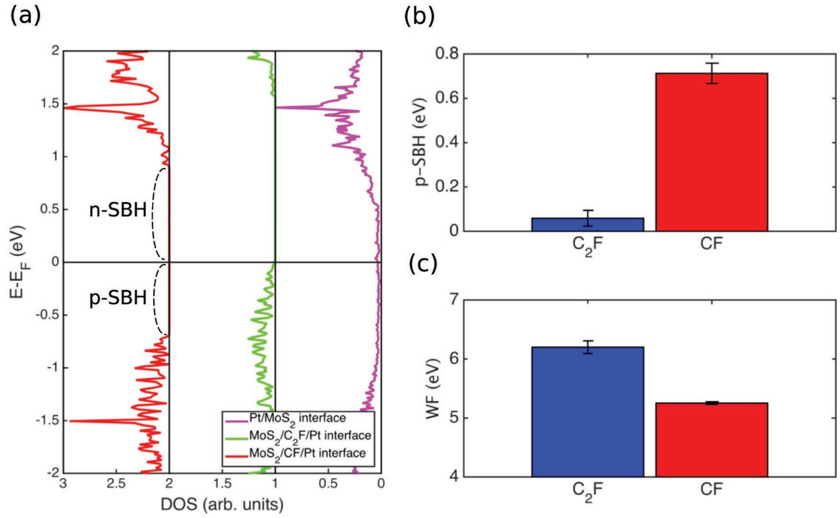

Figure 2. a) Example MoS_2 PDOS plots showing the definition of n-type and p-type SBH. The represented DOS are in the cases when no buffer layer is present, and when GF is inserted between MoS_2 and Pt as C_2F and CF. b) Values of p-SBH for MoS_2/GF/Pt interfaces where GF is present as C_2F and CF. c) Work-function (WF) values of Pt modified by contacting C_2F and CF. In (b) and (c), the results are obtained by averaging three metal-GF-semiconductor structures for each fluorine concentration. The error bars represent the standard error of the mean.

The metal, semiconductor and the buffer layer structures are initially relaxed individually, and then assembled together in the unit cell and relaxed together. Three atomic layers of the metal slab that face the vacuum are held fixed during the relaxation runs to mimic the bulk. In some cases during the relaxation a small number of fluorine atoms detach from the carbon plane. In such cases, the detached fluorine atoms were removed from the cell, and the simulation was run again until a stable structure was obtained. Therefore, our disordered GF structures are slightly off-stoichiometric; C_2F has a mean fluorine concentration of 31.8 ± 1.4 at%, while CF has a mean fluorine concentration of 49.6 ± 0.6 at%. As for the initial distance between the three layers, we choose the one giving the lowest energy in frozen-ion calculations where only the interlayer distance is varied (for more information, see Figures S3 and S4, Supporting Information). The initial distance obtained in this way solely serves to provide a good starting point and improves convergence, as

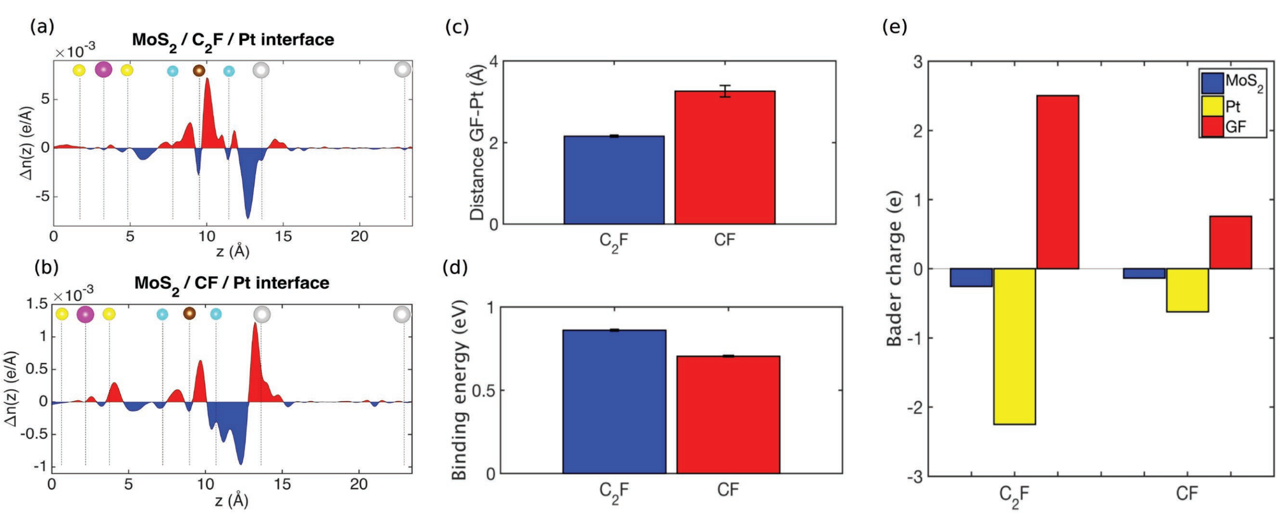

Figure 3. Plots of the plane-averaged electron density difference ($n(z)$) along the z-direction of MoS_2/GF/Pt interface with GF as a) C_2F and b) CF. Color code: red indicates electron accumulation, while blue stands for electron depletion. At the top of each plot, the atomic plane positions are given for reference (see Figure 1 for the atoms' legend). c) Equilibrium distance between GF and Pt after structural relaxation. d) Binding energy (per unit cell) of GF on Pt. e) Bader charges for MoS_2, Pt, and GF. In (c)–(e), all results are shown for GF as C_2F and CF, and are obtained by averaging three metal-GF-semiconductor structures for every fluorine concentration. The error bars represent the standard error of the mean.

the spacing between the layers changes during structural relaxation.

All calculations are performed using plane-wave density functional theory (DFT), as implemented in the Vienna ab initio simulation package (VASP).[36] Core electrons[37,38] are described by the projector-augmented-wave method. We have used the Perdew–Burke–Ernzerhof exchange-correlation functional.[39] Van der Waals (vdW) corrections are considered through the Grimme's DFT-D2 method as implemented in VASP,[40,41] while the spin-orbit interactions are not accounted for here.[14,42] A comparison with other vdW functionals has been carried out, showing no substantial differences (see Figure S5, Supporting Information). We have used an energy cutoff of 500 eV. Atomic positions have been relaxed using the conjugate gradient method, until the residual atomic force on each atom is less than 0.03 eV Å^{-1}. A vacuum region normal to the surface larger than 15 Å is used to avoid interaction between the slab images. A $(5 \times 5 \times 1)$ Γ-centered **k**-point grid is used for structural relaxations, while the **k**-point grid is increased to $(9 \times 9 \times 1)$ to obtain the density of states (DOS). The grid-based Bader method has been used to carry out the charge-density analysis.[43,44]

3. Results and Discussion

For each relaxed metal-GF-semiconductor structure, we computed the DOS in order to obtain the p-SBH, defined as the energy difference between the maximum of the valence band and the Fermi level.[14,45] An example DOS plot is shown in **Figure 2**a. We have adopted the reference-energy method to estimate the p-SBH,[16,21,46] by aligning the semi-core levels of the adsorbed TMD with those of a free-standing TMD layer (see Figure S6 in the Supporting Information for an example). The p-SBH values thus computed are shown in Figure 2b. Our results demonstrate that using C_2F as a buffer layer between MoS_2 and Pt yields a nearly ohmic contact (p-SBH value of 0.06 ± 0.04 eV). Instead, we obtain a larger value of p-SBH (0.71 ± 0.05 eV), upon using CF as a buffer layer. This result is interesting because given the higher concentration of fluorine atoms and consequently, a higher work function value of CF (7.55 eV on average in our calculations) compared to C_2F (6.89 eV on average), one would expect an even lower p-SBH value compared to the case of C_2F, which as it turns out, is not the case.

In order to check the impact of the ordered arrangement of fluorine atoms in the graphene plane on the p-SBH, we computed the p-SBH using CF as a buffer layer in its chair configuration (Figure 5a). We obtained a p-SBH value of 0.55 eV, while the average p-SBH using CF with random attachment of the Fluorine atoms is 0.71 eV, showing that the ordering of fluorine atoms does not result in a dramatic change in the p-SBH value.

In order to understand the physical basis for this result, we investigate the different interfaces involved in greater detail. There are two factors that mainly dictate the value of p-SBH obtained. First, we note that a buffer layer which potentially increases the work function or helps retain the high work function of the metal it is in contact with, would be favorable for forming a p-type contact. Therefore, it is advantageous to have an electron transfer from the metal toward the buffer layer, thereby setting up an interface dipole which could potentially increase the work function. Second, it would be beneficial to have a buffer layer with sufficiently high density of states close to the Fermi level so as to facilitate its pinning. We quantified the charge transfer at the interface by computing the plane-averaged electron density difference $\Delta n(z) = n_{\mathrm{TMD/GF/metal}} - n_{\mathrm{TMD}} - n_{\mathrm{GF}} - n_{\mathrm{metal}}$, where $= n_{\mathrm{TMD/GF/metal}}$ is the total electron density of the three-layer interface, while n_{TMD}, n_{GF} and n_{metal} are those of the individual TMD, GF and metal layers, respectively[45] (see **Figure 3**a,b). First, we notice that the charge redistribution at the TMD/GF interface is weaker compared to the case

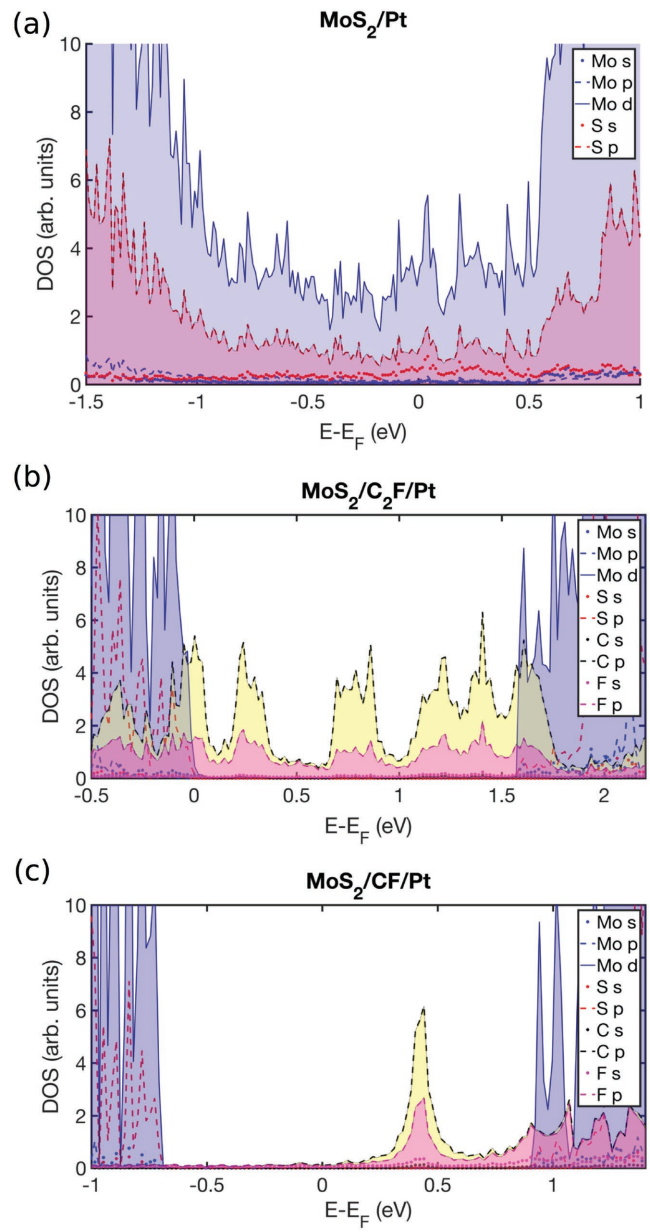

Figure 4. Partial density of states (PDOS) of a) MoS_2/Pt, b) MoS_2/C_2F/Pt, and (c) MoS_2/CF/Pt interfaces. The blue shaded zone in each figure indicates the conduction band and valence band edges, determined by the Mo d-orbitals projection in the band structures. The red shaded area highlights represents the F p-orbitals, while the yellow area denotes the C p-orbitals.

without using the buffer layer (see Figure S7, Supporting Information), confirming that GF is effective in reducing the interaction between the TMD and the metal. We also note that the charge transfer at the GF/Pt interface is generally greater than that at the MoS_2/GF interface, independent of the fluorine concentration. This greater charge transfer taking place between GF and Pt indicates a stronger interaction between them. Our understanding is that the TMD is only physisorbed onto the GF layer,[21,47] and as a result the TMD atomic structures are unperturbed, thereby avoiding the formation of gap states that are known to pin the Fermi level close to the conduction band. We point out that the presence of the buffer layer (GF) would modify the charge transport. Given that the fluorine content is high in the GF layers considered, the buffer layer is expected to be an insulator and charges from the metal would tunnel through to the semiconductor via GF. This transport is expected to be similar to the case when graphene oxide is used as a hole transport layer.

We now turn our attention to the more important metal/GF interface. We observe significant electron transfer at the metal/C_2F interface when compared to the metal/CF interface. Such a notable electron transfer upon contacting Pt with C_2F results in the formation of an interface dipole and consequently, increases the work function of the metal on the C_2F side. We performed additional calculations to compute the value of the resulting work function (see Figure 2c). This was done by relaxing only the Pt/GF (C_2F or CF) structures without the presence of MoS_2 in the unit cell. We found a modified work function value of 6.20 eV in the case of Pt/C_2F, greater than the work function value of Pt (5.30 eV), consistent with the observed electron transfer from the Pt slab toward the C_2F layer.

On the other hand, a weaker charge redistribution at the metal/CF interface results in no considerable changes in the work function of the Pt metal in contact with the CF layer (5.25 eV). Such a difference in charge redistribution between the C_2F and the CF cases can be understood if one considers the chemical interaction between the GF and the metal layers, and their resulting equilibrium geometries. We computed the interfacial binding energies for both GF structures and found the binding energy of CF to be smaller than that of C_2F by 0.16 ± 0.01 eV. These weaker binding energy values are also reflected in the longer equilibrium interlayer distances between the CF and the Pt layers (see Figure 3c,d), thus resulting in a weaker interaction between them. This result helps to understand why we observe a higher value of p-SBH in the case of MoS_2-CF-Pt when compared to the case of MoS_2-C_2F-Pt. It further highlights that increasing the concentration of halogens beyond a certain optimum is unfavorable for obtaining MoS_2-based p-type devices.

While we have shown that charge redistribution is a critical factor controlling the p-SBH values, we proceed to analyze the second factor affecting the interface barrier heights. **Figure 4** shows the partial DOS (PDOS) of the TMD/GF/Pt interfaces, also including the case without the GF buffer layers. First, we notice the presence of gap states of Mo d-orbital character at the MoS_2/Pt interface, as shown in (Figure 4a), consistent with previous work.[14] These gap states of Mo-d orbital character are formed by sulfur-mediated interface hybridization, as explained by Gong et al.[14]

When the buffer layer is introduced, the states of GF and Pt are visible within the band gap of MoS_2, while the gap states of MoS_2 vanish, consistent with our observation of weaker interaction between GF and MoS_2 layers. The states from the GF layer are formed mainly by the C p and F p-orbitals. Further, we notice that these states are delocalized across the entire band gap for the case of C_2F, while they are strongly localized for the case of CF structures. Such strong localization could additionally lead to Fermi level pinning at these states and lead to larger p-SBH values as seen for the case of CF. Therefore, we conclude that, in addition to the primary role played by charge transfer at the interface, the density and the distribution of the localized gap states in GF could play a secondary role in dictating the Fermi level pinning process and thereby control the p-SBH values.

In order to explore the applicability of our findings to other materials, we extend our studies to include a different metal and a different TMD monolayer. We choose to investigate Cobalt (Co) as a metal contact given its high work function combined with low cost. A better lattice match is obtained compared to the case of Pt (see Table ST1, Supporting Information), which is evident from the minimal rearrangement of atoms at the interface as observed in **Figure 5**a,b. The computed p-SBH values are shown in Figure 5c. Again, we obtain a significantly low p-SBH value of 0.12 eV upon using Co in conjunction with C_2F as a buffer layer. Qualitatively, as compared to the Pt metal contact, we find no differences in the MoS_2 p-SBH values upon using Co as a metal contact, demonstrating that our analysis of the interfaces above (with Pt) is extendable to other metal contacts as well.

Finally, we have considered the case of a small work-function TMD, instead of MoS_2. The TMD with the smallest work-function is WTe_2, but its only stable phase is the distorted octahedral structure, which is semi-metallic.[6] Since we require a semiconductor, we have chosen to study WSe_2 instead, which has shown significant promise toward realizing p-type FETs.[20,48]

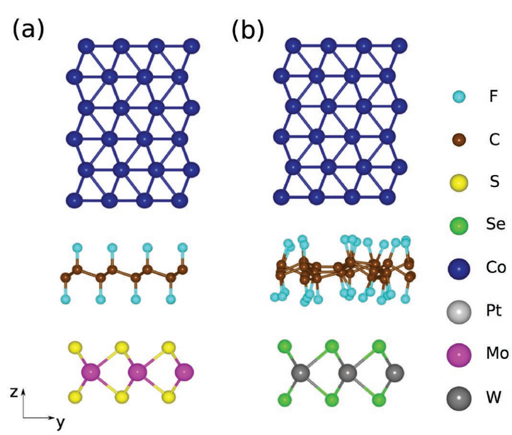

(c)

System	p-SBH (eV)
$MoS_2/C_2F/Co$	0.12
MoS_2/CF/Co	0.41
$WSe_2/C_2F/Co$	0.08
WSe_2/CF/Co	0.04

Figure 5. Example of relaxed supercells (lateral view) formed by a) MoS_2/CF/Co and b) WSe_2/CF/Co. In (a), CF is in the chair configuration. c) Values of p-SBH using Co as the contact metal, in the case of MoS_2 and WSe_2 structures with C_2F and CF as buffer layers.

Interestingly, we find that the interfaces formed by WSe_2/GF/Pt possess ohmic character, with a negligible p-SBH, for both C_2F and CF cases. The values of the p-SB using Co as a metal contact are also shown in Figure 5c, which are again observed to be very low (<0.1 eV). The charge difference and PDOS analysis (see Figures S8 and S9, Supporting Information) of the WSe_2/GF/Pt interfaces show similar trends to the MoS_2 case, although evidently these changes do not impact the p-SBH values given the low work function of WSe_2. Thus, for low work function TMDs, we find that both C_2F and CF could function as efficient hole injection layers, unlike in the case of MoS_2.

4. Conclusion

We propose and study graphene fluoride (GF) as an efficient hole-injection layer for TMD-based electronic devices. Ab initio simulations have been used to model TMD/GF/metallic interfaces. For high work function TMDs such as MoS_2, we demonstrate a nearly p-type ohmic contact using C_2F as the buffer layer, while instead we show that CF leads to a significant p-type SBH value. This shows that there exists an optimal value of the halogen concentration beyond which the buffer layer fails to perform as an efficient hole injection layer. Our analysis shows that the p-SBH value is strongly controlled by the charge redistribution at the metal/GF interface, which in turn is affected by the chemical interaction and equilibrium geometry of the metal/GF interface. On the other hand, for low work function TMDs such as WSe_2, a p-type ohmic contact is obtained for both C_2F and CF buffer layers. Our results demonstrate the potential of functionalized graphenes as buffer layers and open up an exciting pathway to obtain all-2D material TMD-based p-type electronic devices.

Supporting Information

Supporting Information is available from the Wiley Online Library or from the author.

Acknowledgements

The authors acknowledge the use of the Finnish CSC-IT Center for Sciences supercomputing resources. T.M. acknowledges financial support from the Academy of Finland through its Centres of Excellence Programme (2012–2017) under Project No. 251748 and The Finnish Academy of Science and Letters, Vilho, Yrjö, and Kalle Väisälä Foundation. P.V.K. and J.C.G. are grateful for financial support from the Eni Solar Frontiers Program at MIT. T.M. performed all the calculations, analyzed the results, and wrote the manuscript. P.V.K. assisted with analyzing the results and writing the manuscript. J.C.G. and A.F. supervised the entire project and assisted in manuscript preparation. All authors discussed the results and commented on the manuscript.

Keywords

graphene fluoride, hole injection layers, MoS_2, p-type FETs, WSe_2

Received: August 12, 2016
Revised: February 7, 2017
Published online:

[1] B. Radisavljevic, M. B. Whitwick, A. Kis, *ACS Nano* **2011**, *5*, 9934.
[2] Y. Yoon, K. Ganapathi, S. Salahuddin, *Nano Lett.* **2011**, *11*, 3768.
[3] S. Das, H.-Y. Chen, A. V. Penumatcha, J. Appenzeller, *Nano Lett.* **2013**, *13*, 100.
[4] B. Radisavljevic, A. Radenovic, J. Brivio, V. Giacometti, A. Kis, *Nat. Nanotechnol.* **2011**, *6*, 147.
[5] W. Bao, X. Cai, D. Kim, K. Sridhara, K. Fuhrer, *Appl. Phys. Lett.* **2013**, 102.
[6] J. Kang, S. Tongay, J. Zhou, J. Li, J. Wu, *Appl. Phys. Lett.* **2013**, *102*.
[7] Q. H. Wang, K. Kalantar-Zadeh, A. Kis, J. N. Coleman, M. S. Strano, *Nat. Nanotechnol.* **2012**, *7*, 699.
[8] C. Kuan-Chang, Z. Xin-Quan, L. Xiaoze, M. Vinod, C. Yung-Fu, W. Jenn-Ming, L. Yi-Hsien, *IEEE J. Quantum Electron.* **2015**, *51*, 0600110.
[9] F Schwierz, *Nat. Nanotechnol.* **2011**, *6*, 135.
[10] F. Schwierz, *Nat. Nanotechnol.* **2010**, *5*, 487.
[11] B. Radisavljevic, A. Kis, *Nature Mater.* **2013**, *12*, 815.
[12] C.-J. Shih, Q. H. Wang, Y. Son, Z. Jin, D. Blankschtein, M. S. Strano, *ACS Nano* **2014**, *8*, 5790.
[13] S. Chuang, C. Battaglia, A. Azcatl, S. McDonnell, J. S. Kang, X. Yin, M. Tosun, R. Kapadia, H. Fang, M. Wallace, A. Javey, *Nano Lett.* **2014**, *14*, 1337.
[14] C. Gong, L. Colombo, R. M. Wallace, K. Cho, *Nano Lett.* **2014**, *14*, 1714.
[15] Y. Liu, P. Stradins, S.-H. Wei, *Sci. Adv.* **2016**, *2*, e1600069.
[16] Y. Guo, D. Liu, J. Robertson, *ACS Appl. Mater. Interfaces* **2015**, *7*, 25709.
[17] L. Francois, T. A. Alec, *Nat. Nano* **2011**, *6*, 773.
[18] S. McDonnell, R. Addou, C. Buie, R. Wallace, C. L. Hinkle, *ACS Nano* **2014**, *8*, 2880.
[19] S. McDonnell, A. Azcatl, R. Addou, C. Gong, C. Battaglia, S. Chuang, K. Cho, A. Javey, R. M. Wallace, *ACS Nano* **2014**, *8*, 6265.
[20] H. Fang, S. Chuang, T. C. Chang, K. Takei, T. Takahashi, A. Javey, *Nano Lett.* **2012**, *12*, 3788.
[21] M. Farmanbar, G. Brocks, *Adv. Electron. Mater.* **2016**, *2*, 1500405.
[22] W. Park, Y. Kim, S. K. Lee, U. Jung, J. H. Yang, C. Cho, Y. J. Kim, S. K. Lim, I. S. Hwang, H. B. R. Lee, B. H. Lee, *IEEE Int. Electron Devices Meet.* **2014**, *14*, 511.
[23] B. Shubhadeep, L. G. Kolla, N. Digbijoy, B. Navakanta, *IEEE Trans. Electron Devices* **2016**, *63*, 2556.
[24] Y. Ding, Y. Wang, J. Ni, L. Shi, S. Shi, W. Tang, *Phys. B* **2011**, *406*, 2254.
[25] T. Musso, P. V. Kumar, A. S. Foster, J. C. Grossman, *ACS Nano* **2014**, *8*, 11432.
[26] M. A. Khan, S. Rathi, I. Lee, L. Li, D. Lim, M. Kang, G. H. Kim, *Appl. Phys. Lett.* **2016**, *108*, 093104.
[27] F. Karlick, K. K. R. Datta, M. Otyepka, R. Zboil, *ACS Nano* **2013**, *7*, 6434.
[28] A. Bagri, C. Mattevi, M. Acik, Y. J. Chabal, M. Chhowalla, V. B. Shenoy, *Nat. Chem.* **2010**, *2*, 581.
[29] R. R. Nair, W. Ren, R. Jalil, I. Riaz, V. G. Kravets, L. Britnell, P. Blake, F. Schedin, A. S. Mayorov, S. Yuan, M. I. Katsnelson, H. M. Cheng, W. Strupinski, L. G. Bulusheva, A. V. Okotrub, I. V. Grigorieva, A. N. Grigorenko, K. S. Novoselov, A. K. Geim, *Small* **2010**, *6*, 2877.
[30] F. Karlick, R. Zboil, M. Otyepka, *J. Chem. Phys.* **2012**, *137*.
[31] S. S. Han, T. H. Yu, B. V. Merinov, A. C. T. van Duin, R. Yazami, A. William, I. Goddard, *Chem. Mater.* **2010**, *22*, 2142.
[32] J. T. Robinson, J. S. Burgess, C. E. Junkermeier, S. C. Badescu, T. L. Reinecke, F. K. Perkins, M. K. Zalalutdniov, J. W. Baldwin, J. C. Culbertson, P. E. Sheehan, E. S. Snow, *Nano Lett.* **2010**, *10*, 3001.
[33] J.-C. Charlier, X. Gonze, J.-P. Michenaud, *Phys. Rev. B* **1993**, *47*, 16162.

[34] O. Leenaerts, H. Peelaers, A. D. Hernández-Nieves, B. Partoens, F. M. Peeters, *Phys. Rev. B* **2010**, *82*, 195436.
[35] Y. Ma, Y. Dai, M. Guo, C. Niu, B. Huang, *Nanoscale* **2011**, *3*, 3883.
[36] G. Kresse, J. Furthmüller, *Phys. Rev. B* **1996**, *54*, 11169.
[37] P. E. Blöchl, *Phys. Rev. B* **1994**, *50*, 17953.
[38] G. Kresse, D. Joubert, *Phys. Rev. B* **1999**, *59*, 1758.
[39] J. P. Perdew, K. Burke, M. Ernzerhof, *Phys. Rev. Lett.* **1996**, *77*, 3865.
[40] S. Grimme, *J. Comput. Chem.* **2006**, *27*, 1787.
[41] T. Bucko, J. Hafner, S. Lebègue, J. G. Angyan, *J. Phys. Chem. A* **2010**, *114*, 11814.
[42] I. Popov, G. Seifert, D. Tomànek, *Phys. Rev. Lett.* **2012**, *108*, 156802.
[43] G. Henkelman, A. Arnaldsson, H. Jónsson, *Comput. Mater. Sci.* **2006**, *36*, 354.
[44] W. Tang, E. Sanville, G. Henkelman, *J. Phys.: Condens. Matter* **2009**, *21*, 084204.
[45] L.-Y. Gan, Y.-J. Zhao, D. Huang, U. Schwingenschlögl, *Phys. Rev. B* **2013**, *87*, 245307.
[46] M. Farmanbar, G. Brocks, *Phys. Rev. B* **2016**, *93*, 085304.
[47] W. S. Leong, X. Luo, Y. Li, K. H. Khoo, S. Y. Quek, J. T. L. Thong, *ACS Nano* **2015**, *9*, 869.
[48] H.-J. Chuang, B. Chamlagain, M. Koehler, M. M. Perera, J. Yan, D. Mandrus, D. Tomnek, Z. Zhou, *Nano Lett.* **2016**, *16*, 1896.